2008-02-07

A Model for Predicting the Piezoresistive Effect in Microflexures Experiencing Bending and Tension Loads

Gary K. Johns
garykjohns@gmail.com

Larry L. Howell
lhowell@byu.edu

Brian D. Jensen

Timothy W. McLain
mclain@byu.edu

Original Publication Citation

Johns, G.K., Howell, L.L., Jensen, B.D., McLain, T.W., "A Model for Predicting the Piezoresistive Effect in Microflexures Experiencing Bending and Tension Loads," Journal of Microelectromechanical Systems, Vol. 17, No. 1, pp. 226-235, 28

A Model for Predicting the Piezoresistive Effect in Microflexures Experiencing Bending and Tension Loads

Gary K. Johns, Larry L. Howell, *Fellow, ASME*, Brian D. Jensen, *Member, ASME*, and Timothy W. McLain, *Senior Member, IEEE*

***Abstract*—This paper proposes a model for predicting the piezoresistive effect in microflexures experiencing bending stresses. Linear models have long existed for describing piezoresistivity for members in pure tension and compression. However, extensions of linear models to more complex loading conditions do not match with experimental results. A second-order model to predict piezoresistive effects in tension, compression, and more complex loading conditions is proposed. A reduced form of the general second-order model is presented for thin flexures in bending. A three-step approach is used to determine the piezoresistive coefficients for this reduced-form model. The approach is demonstrated for two sets of n-type polysilicon. The predictive ability of the model is investigated by comparing the results to the experimental results using the new piezoresistive model and coefficients. One of the ways to implement the model is with multiphysics finite element analysis (FEA). The piezoresistive FEA for flexures algorithm is a FEA implementation of the unidirectional form of the model for flexures. The results presented in this paper are for the simplified cases of long thin flexures experiencing bending and axial loads. This new model could contribute to optimized sensors and feedback control of microdevices, nanopositioning, and self-sensing microdevices. [2007-0052]**

***Index Terms*—Finite element methods, microelectromechanical devices, microsensors, modeling, piezoresistance, piezoresistive devices.**

I. Introduction

INTEGRATED piezoresistive self-sensing is a sensing method that utilizes the deflection of intrinsic microflexures to sense the state of a microdevice [1]–[4]. These microflexures deform under a force or displacement caused by a physical phenomenon. Due to their piezoresistive material property, the electrical resistance of a flexure changes in correlation with its deformation. This change in resistance can be used to calculate the value of the original force or displacement. Piezoresistive elements have often been implemented in microsystems in ways that place the piezoresistive elements in pure tension or compression (such as on the surface of a beam or a membrane). In the proposed integrated piezoresistive self-sensing devices, however, rather than the piezoresistive element being part of the flexure, it is the flexure. The loading conditions for such sensors are more complex than pure tension or compression.

This paper shows that analytical resistance data from the current model of piezoresistivity do not match with the experimental data for microflexures in bending, and introduces a second-order model to predict the piezoresistive effect under more complex loading conditions. This model is demonstrated by determining the piezoresistive coefficients for n-type polycrystalline silicon. The model and resulting piezoresistive coefficients are used in a case study to model the piezoresistive behavior of two microdevices.

II. Background

Piezoresistivity is a material property that couples mechanical strain to bulk electrical resistivity [5]. In other words, if a piezoresistive member is bent, stretched, or compressed, its electrical resistance changes. The change in resistance can then be measured or converted into a change in voltage, and the corresponding stress (or strain) can be determined. Thus, stresses and strains can be related to a physical phenomenon such as displacement or applied force through piezoresistivity [6].

Currently, the piezoresistive effect is most widely used in various types of sensors. Sensors utilizing the piezoresistive effect include microphones, pressure sensors, force sensors, flow sensors, and displacement sensors [7], [8]. One of the most common techniques for fabricating piezoresistive sensors is to diffuse a resistor onto a silicon diaphragm or cantilever beam that deflects in reaction to an external stimulus [9], [10]. The diffused silicon resistor is put into tension or compression as the diaphragm or cantilever deflects. The resistance elements that formed from the diffused silicon can be electrically connected in a Wheatstone bridge configuration. The change in resistance is then measured directly from a change in voltage.

Many microdevices are compliant mechanisms [11], which gain some of their mobility from deflection rather than pin joints or other hinges. Compliant devices are particularly advantageous at the microlevel because they can be fabricated in a single layer and require no assembly. Compliant mechanisms also avoid the friction, wear, and backlash that are inherent in joints with rubbing parts. As compliant beams (flexures) are

Manuscript received February 28, 2007; revised October 3, 2007. Subject Editor H. Fujita.

G. K. Johns was with the Department of Mechanical Engineering, Brigham Young University, Provo, UT 84602 USA. He is now with Merit Sensor Systems, Inc., South Jordan, UT 84095 USA.

L. L. Howell, B. D. Jensen, and T. W. McLain are with the Department of Mechanical Engineering, Brigham Young University, Provo, UT 84602 USA.

Color versions of one or more of the figures in this paper are available online at http://ieeexplore.ieee.org.

Digital Object Identifier 10.1109/JMEMS.2007.911874

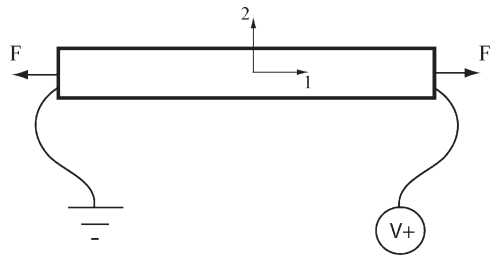

Fig. 1. Schematic of Charles Smith's experimental setup. Coordinate axis 3 is into the page.

deflected, their stress–strain state is changed, and thus, they are well suited for integrated piezoresistive sensors.

A. Linear Model of Piezoresistivity

In 1954, Charles Smith published a paper [12] exposing the piezoresistive properties of silicon and germanium. Experimental data were gathered and used to derive the piezoresistive coefficients that relate change in resistance to stress. The experimental setup is shown in Fig. 1. A beam was put in tension, and the change in electrical resistance was measured. These data were used to calculate the piezoresistive coefficient π_{11} as

$$\pi_{11} = \frac{1}{S}\frac{\Delta R}{R_0} \tag{1}$$

where S denotes stress, and R is the electrical resistance. It was also found that silicon and germanium are much more sensitive to the piezoresistive effect than most metals.

The fractional change in resistivity is related to stress through the Π matrix, which is shown in a simplified form for the cubic crystal structure of silicon as

$$\frac{1}{\rho}\begin{bmatrix}\Delta\rho_1\\ \Delta\rho_2\\ \Delta\rho_3\\ \Delta\rho_4\\ \Delta\rho_5\\ \Delta\rho_6\end{bmatrix} = \begin{bmatrix}\pi_{11} & \pi_{12} & \pi_{12} & 0 & 0 & 0\\ \pi_{12} & \pi_{11} & \pi_{12} & 0 & 0 & 0\\ \pi_{12} & \pi_{12} & \pi_{11} & 0 & 0 & 0\\ 0 & 0 & 0 & \pi_{44} & 0 & 0\\ 0 & 0 & 0 & 0 & \pi_{44} & 0\\ 0 & 0 & 0 & 0 & 0 & \pi_{44}\end{bmatrix}\begin{bmatrix}\sigma_1\\ \sigma_2\\ \sigma_3\\ \tau_{12}\\ \tau_{13}\\ \tau_{23}\end{bmatrix} \tag{2}$$

where ρ is the original resistivity, and $\Delta\rho_i$ is the change in resistivity in the i^{th} direction. The terms σ_1, σ_2, and σ_3 are the stresses along the axes of interest, while τ_{12}, τ_{13}, and τ_{23} are the shear stresses. The elements of the Π matrix are referred to as piezoresistive (π) coefficients. Defining subscript 1 to represent the direction along the length of a long thin flexure, an equation can be written for the fractional change in resistivity in that direction as

$$\frac{\Delta\rho_1}{\rho} = \pi_{11}\sigma_1 + \pi_{12}\sigma_2 + \pi_{12}\sigma_3. \tag{3}$$

Notice that (3) is not a function of shear stress. In addition, for beams bending in plane, the stress in the direction along the length of the beam is much greater than the stresses in the other two orthogonal directions. By assuming that these lower stresses are insignificant, (3) simplifies to

$$\frac{\Delta\rho_1}{\rho} = \pi_{11}\sigma_1. \tag{4}$$

This model works well when modeling beams loaded in pure tension or compression and for piezoresistive elements on one surface of a membrane where they are in pure tension or compression. However, it will be shown that these models are not adequate for more complex loading conditions.

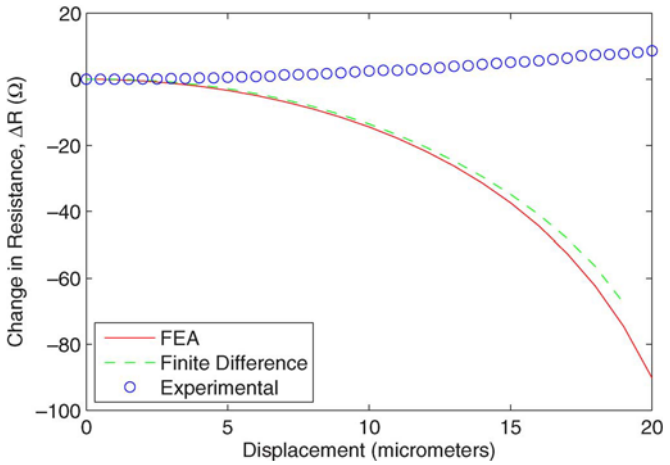

Fig. 2. Analytical results and experimental data comparison of the superposition model [13]. The nominal resistance of the experimental device is 2266 Ω.

B. Superposition Model of Piezoresistivity in Bending

Beams in bending simultaneously experience different levels of tension and compression throughout their cross sections and along their lengths. Smith's linear model was considered as a possible method for predicting the piezoresistive effect in beams undergoing bending because it has been shown to predict the change in resistance of beams in tension or compression. A superposition form of the linear model was used to calculate separately the change in resistivity for the tensile and compressive segments of the beam. The principle of superposition was used to add these components together. To check the validity of the superposition model, resistance-deflection curves predicting the change in resistance of beams under a bending load were used. An n-type polysilicon device was used for comparing model predictions to experimental results. This investigation is further described in [13] and [14].

The superposition model was applied to bending using commercial finite element analysis (FEA) and custom finite-difference models. Each method produced a negative-sloped nonlinear curve, whereas every experimental result for bending produced a positive-sloped nonlinear curve, as shown in Fig. 2. The nature of Smith's model precludes a positive-sloped nonlinear resistance curve for a flexure in bending due to the way resistors in parallel combine [13], [14].

These results show that a superposition form of the linear piezoresistance model failed to predict the trend and the magnitude of the piezoresistive effect for the simple bending device.

The model predicts a decrease in resistance due to bending stresses regardless of the sign or value of the piezoresistance coefficients used in the analysis. Therefore, a model of piezoresistance, which can predict the piezoresistive effect on more complex loading conditions such as bending and combined loads, is needed. A model like the one described would aid in the design, optimization, and implementation of integral piezoresistive sensors. This model may also yield insights into the physical phenomenon behind the piezoresistive effect.

III. Proposed Model for Piezoresistivity in Bending

For a new piezoresistive model to be of the most use, it must be able to predict the change in resistance for the conditions covered by Smith's linear model (pure tension and compression) as well as for other loading conditions, including bending. Such a model would be valuable in analyzing piezoresistive microsensors that employ flexures.

A. General Form

A second-order model has been developed, which expands upon the linear model by adding the ability to analyze loading conditions other than pure tension and compression. In its most general form, it adds second-order stress terms to the existing model. A matrix expression of the model (5) is shown at the bottom of the page. The diagonal elements denoted by S are

$$S = [\sigma_1 \quad \sigma_2 \quad \sigma_3 \quad \tau_{12} \quad \tau_{13} \quad \tau_{23}]. \tag{6}$$

The diagonal elements of the new Π matrix, called the Π^* matrix, are represented by

$$P = \begin{bmatrix} \pi_{11}^* & \pi_{12}^* & \pi_{13}^* & \pi_{14}^* & \pi_{15}^* & \pi_{16}^* \\ \pi_{21}^* & \pi_{22}^* & \pi_{23}^* & \pi_{24}^* & \pi_{25}^* & \pi_{26}^* \\ \pi_{31}^* & \pi_{32}^* & \pi_{33}^* & \pi_{34}^* & \pi_{35}^* & \pi_{36}^* \\ \pi_{41}^* & \pi_{42}^* & \pi_{43}^* & \pi_{44}^* & \pi_{45}^* & \pi_{46}^* \\ \pi_{51}^* & \pi_{52}^* & \pi_{53}^* & \pi_{54}^* & \pi_{55}^* & \pi_{56}^* \\ \pi_{61}^* & \pi_{62}^* & \pi_{63}^* & \pi_{64}^* & \pi_{65}^* & \pi_{66}^* \end{bmatrix}. \tag{7}$$

These equations could also be done in tensorial form, such as that used in [15]. Substituting (6) into (5) expands the stress matrices to 6×36 and 36×6. Substituting (7) into the Π^* matrix results in a 36×36 matrix. In this general form, there are 252 unknown π and π^* coefficients. This general model yields the fractional change in resistivity in all primary and cross directions.

B. Unidirectional Form for Flexures

The general model of (5) can be simplified for long thin flexures which are the elements of most concern for compliant microdevices and are also the focus of this research. For microflexures, the majority of the electrical current is along its length. As the flexures are bent, there will be a component of current across the beam, but it will be insignificant compared to the current along its length. Therefore, the fractional change in resistivity will also be greatest along the length of the beam. A simplified version of the general model is prepared for this specific case.

Since the direction of interest is along the beam, the 1 direction is defined to be along the length of the beam. Therefore, only the first row of the general equation is necessary for the model. This corresponds with an in-plane stress of an isotropic material. Note that σ_3, τ_{13}, and τ_{23} will drop out of the equation because it is constrained to in-plane displacements. The new simplified model then includes nine piezoresistive coefficients mapping to two primary stresses (σ_1 and σ_2), the shear stress (τ_{12}), each stress squared (σ_1^2, σ_2^2, and τ_{12}^2), and the crosses between the stresses ($\sigma_1\sigma_2$, $\sigma_1\tau_{12}$, and $\sigma_2\tau_{12}$). The unidirectional form of the new model is

$$\frac{\Delta\rho_1}{\rho_0} = \sigma_1\pi_{11} + \sigma_2\pi_{12} + \tau_{12}\pi_{13} + \sigma_1^2\pi_{21}^* + \sigma_2^2\pi_{22}^* + \tau_{12}^2\pi_{23}^* + \sigma_1\sigma_2\pi_{24}^* + \sigma_1\tau_{12}\pi_{25}^* + \sigma_2\tau_{12}\pi_{26}^* \tag{8}$$

where the first three terms are similar to those used in Smith's linear model, i.e., they are each the product of an individual stress term and the corresponding piezoresistive coefficient.

A sensitivity analysis was used to determine which coefficients were significant for predicting the piezoresistive effect of thin flexures in bending. Two of the nine coefficients were shown to have the largest effect on the result. The two most important coefficients were those associated with σ_1 and σ_1^2.

$$\frac{1}{\rho}\begin{bmatrix} \Delta\rho_1 \\ \Delta\rho_2 \\ \Delta\rho_3 \\ \Delta\rho_4 \\ \Delta\rho_5 \\ \Delta\rho_6 \end{bmatrix} = \begin{bmatrix} \pi_{11} & \pi_{12} & \pi_{13} & \pi_{14} & \pi_{15} & \pi_{16} \\ \pi_{21} & \pi_{22} & \pi_{23} & \pi_{24} & \pi_{25} & \pi_{26} \\ \pi_{31} & \pi_{32} & \pi_{33} & \pi_{34} & \pi_{35} & \pi_{36} \\ \pi_{41} & \pi_{42} & \pi_{43} & \pi_{44} & \pi_{45} & \pi_{46} \\ \pi_{51} & \pi_{52} & \pi_{53} & \pi_{54} & \pi_{55} & \pi_{56} \\ \pi_{61} & \pi_{62} & \pi_{63} & \pi_{64} & \pi_{65} & \pi_{66} \end{bmatrix} \begin{bmatrix} \sigma_1 \\ \sigma_2 \\ \sigma_3 \\ \tau_{12} \\ \tau_{13} \\ \tau_{23} \end{bmatrix} \cdots + \operatorname{diag}\left(\begin{bmatrix} S & 0 & 0 & 0 & 0 & 0 \\ 0 & S & 0 & 0 & 0 & 0 \\ 0 & 0 & S & 0 & 0 & 0 \\ 0 & 0 & 0 & S & 0 & 0 \\ 0 & 0 & 0 & 0 & S & 0 \\ 0 & 0 & 0 & 0 & 0 & S \end{bmatrix} \begin{bmatrix} P & 0 & 0 & 0 & 0 & 0 \\ 0 & P & 0 & 0 & 0 & 0 \\ 0 & 0 & P & 0 & 0 & 0 \\ 0 & 0 & 0 & P & 0 & 0 \\ 0 & 0 & 0 & 0 & P & 0 \\ 0 & 0 & 0 & 0 & 0 & P \end{bmatrix} \begin{bmatrix} S^T & 0 & 0 & 0 & 0 & 0 \\ 0 & S^T & 0 & 0 & 0 & 0 \\ 0 & 0 & S^T & 0 & 0 & 0 \\ 0 & 0 & 0 & S^T & 0 & 0 \\ 0 & 0 & 0 & 0 & S^T & 0 \\ 0 & 0 & 0 & 0 & 0 & S^T \end{bmatrix} \right) \tag{5}$$

This was not surprising considering that shear and off-axis stresses are small for thin flexures in bending. Eliminating all but these two terms results in a reduced model in the form

$$\frac{\Delta\rho_1}{\rho} = \sigma_1\pi_{11} + \sigma_1^2\pi_{21}^*. \tag{9}$$

IV. Determining Piezoresistive Coefficients

Values of piezoresistive coefficients are influenced by many factors and can be difficult to determine. Many researchers have studied how gauge factors $(\Delta R/R\epsilon)$ or linear piezoresistive coefficients (those used in the linear model) vary with changes in an influencing factor (see [16]–[25]). Some of these factors include the following:

1) temperature;
2) original bulk resistivity;
3) dopant type;
4) dopant concentration;
5) crystalline structure;
6) mono- or polysilicon structure;
7) surface concentration of a diffused layer.

All of these factors contribute to the difficulty in finding accurate piezoresistive coefficients. However, having accurate coefficients is imperative to adequately model sensors. This is due to the intrinsic coupling of resistivity and stress in piezoresistive materials. This section describes a three-step process that can be used to determine the values of the piezoresistive coefficients in the unidirectional form of the new model.

Step 1) Gather empirical resistance data from test devices.
Step 2) Calculate analytical data using the unidirectional form of the model.
Step 3) Optimize the piezoresistive coefficients to minimize the difference between the empirical data and the analytical data.

Each of these steps is described in more detail in the following sections, and they are demonstrated by employing the approach to determine the piezoresistive coefficients for two materials with different piezoresistive properties: MUMPs[1] poly 1 and MUMPs poly 2 (the first and second free layers of the MUMPs fabrication process). Once the piezoresistive coefficients are determined from test structures, they may be used in modeling the behavior of other devices and in device design.

A. Step 1—Empirical Data

The first step in the process is to gather empirical data from test devices. To demonstrate this step, two types of devices were used: a tension device (Fig. 3) and a bending device (Fig. 4). Each device was fabricated in both the poly 1 and the poly 2 layers, making four test devices. Specifications for the four devices used are given in Table I. Device names, such as Ten50p1, represent a tension device made from poly 1 with 50-μm length legs.

[1]MUMPs is a prototype fabrication process for surface micromachined MEMS [26].

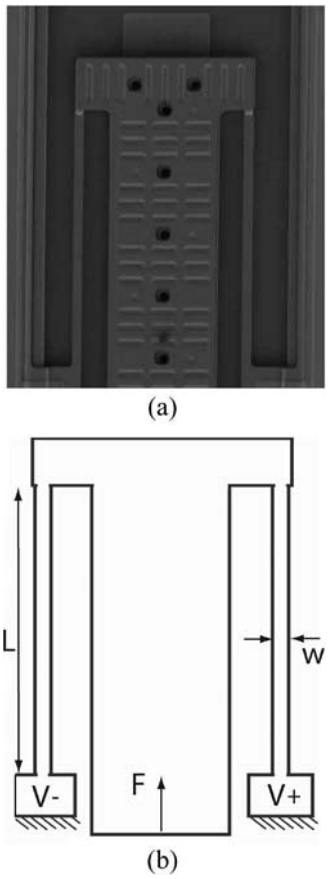

Fig. 3. (a) SEM and (b) schematic of tension microdevice.

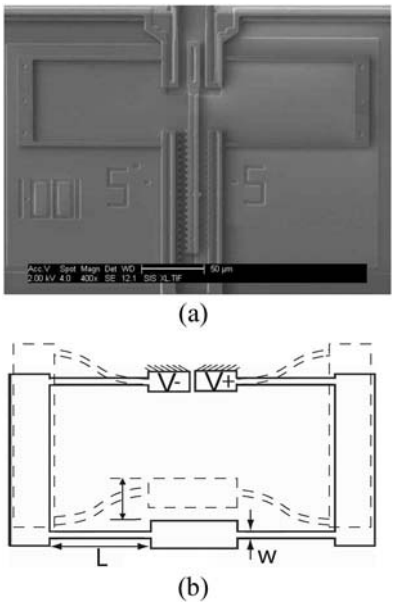

Fig. 4. (a) SEM and (b) schematic of bending microdevice.

Each of these devices was fabricated with a probe guide and a force gauge [27] or optical vernier, as shown in Fig. 5, to facilitate application and measurement of forces or displacements. The probe guide is a parallel-guided mechanism with a large enclosure to accept a probe tip. The design resists off-axis forces leading to a more direct applied force. In the tension

TABLE I
DIMENSIONS FOR MICRODEVICES ARE GIVEN IN MICROMETERS

Device Name	Fabrication Method	Member Length, L	In-Plane Width, w	Out-of-Plane Thickness, t	Polysilicon Layer
Ten50p1	MUMPs	50	3	2	1
Ten100p2	MUMPs	100	3	1.5	2
Ben100p1	MUMPs	100	3	2	1
Ben100p2	MUMPs	100	3	1.5	2

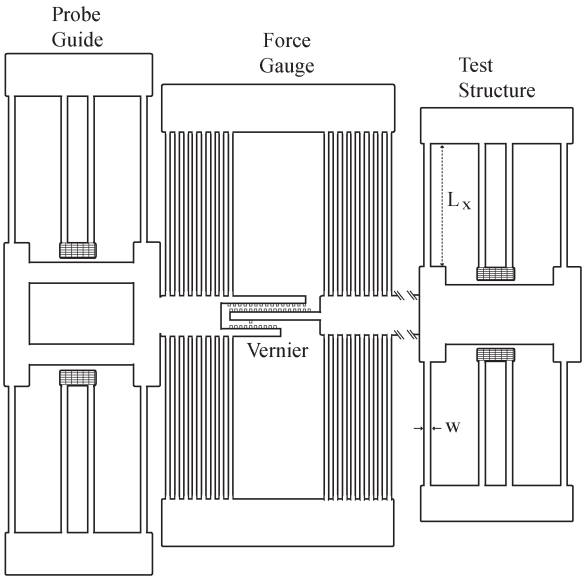

Fig. 5. Each test structure included a microprobe guide (left) and a linear force gauge (center).

device setup, the probe guide is directly connected to the force gauge. The force gauge is also a parallel-guided mechanism with a known spring constant. By using this spring constant and the optical vernier, the force can be directly calculated. The optical vernier consists of an opposing set of teeth. There is a direct correlation between displacement and teeth alignment. Each sequential alignment of a set of teeth represents a 0.5-μm displacement. These components enabled accurate measurements for the tests.

After the devices were mechanically released, a wedge bonder was used to attach gold wires to their bond pads, which are electrically connected through the deflecting flexures of the device. Testing began by applying forces to the tension devices and displacements to the bending devices. Data were obtained by measuring the resistance across their bond pads for each force or displacement. For the tension device, an optical vernier on the force gauge was used to obtain the displacements of the force gauge. The forces were then calculated using large deflection equations [11]. For the bending device, the optical vernier was directly used to obtain displacement data. The data for the tension device were used to produce change in resistance versus stress curves, whereas the data for the bending device produced change in resistance versus displacement curves. These curves will be referred to as empirical data curves and are shown in Figs. 6 and 7. Note that the tension data are nearly linear with a negative slope, which is consistent with the predictions made by Smith's model. The bending data, however, have a trend not predicted by the previous models.

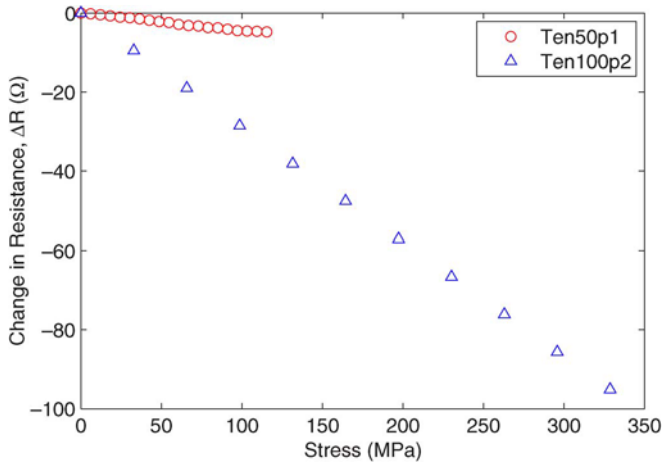

Fig. 6. Experimental data for MUMPs poly 1 and poly 2 in tension. The nominal resistances for Ten50p1 and Ten100p2 are 450 and 2400 Ω, respectively.

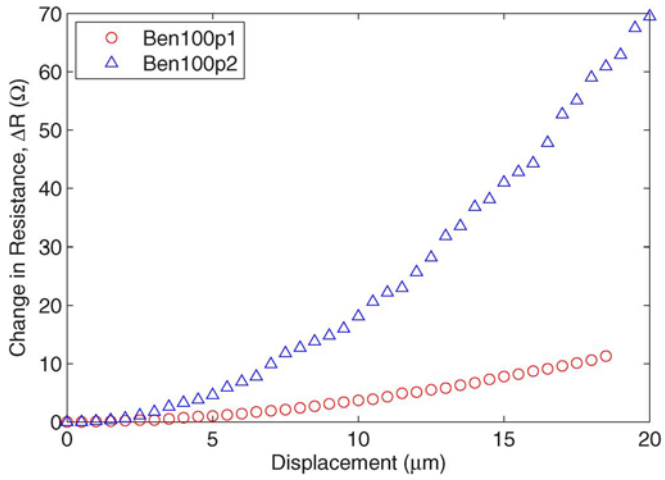

Fig. 7. Experimental data for MUMPs poly 1 and poly 2 in bending. The nominal resistances for Ben100p1 and Ben100p2 are 2266 and 5175 Ω, respectively.

B. Step 2—Analytical Data

The second step is to use the unidirectional form of the model to produce the calculated data from which the analytical data curves are produced. This was done with the piezoresistive FEA for flexures (PFF) algorithm. The PFF algorithm was developed to implement the unidirectional form of the model. It requires both electrical and mechanical capabilities (including nonlinear analysis) to predict the piezoresistive effect in isotropic flexures experiencing in-plane stresses. A commercial FEA code, ANSYS, was used because of its capabilities in these areas. An outline of the algorithm implementation is given in the following with specifications for the flexure shown in Fig. 8 and Table II. The element size listed in Table II resulted in models of 420 elements for a half model of the tension device and 1670 elements for an eighth model of the bending device. The ANSYS analysis was a 2-D nonlinear analysis with in-plane bending and tension loads applied. In the models, one end of the beam was constrained, whereas the load was applied on the other end. The load was applied across the end of the tension beams and as a point load on the top corner of

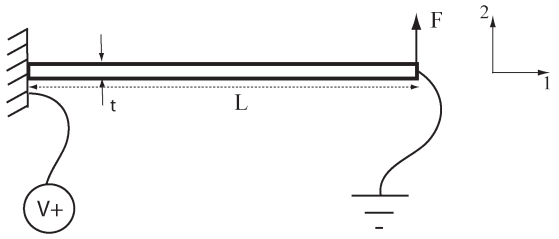

Fig. 8. Example schematic of model for PFF algorithm. Coordinate axis 3 is into the page.

TABLE II
INPUT PARAMETERS FOR PFF ALGORITHM [14]

Parameter	Value	Units
Length (L)	50	μm
Width (w)	3	μm
Thickness (t)	2	μm
Modulus	164000	MPa
Poisson's Ratio	0.23	-
Load steps	20	-
Displacement	10	μm
Tolerance ($\frac{\Delta R}{R}$)	0.0001	-
Resistivity	2.77e-5	Ω-m
Applied Voltage	3	V
Ground Voltage	0	V
π_{11}	-1.1876e-4	MPa^{-1}
π_{21}	4.3125e-8	MPa^{-2}
Mech. Element	Plane82	-
Elec. Element	Plane230	-
Element size	0.3	μm

the bending beams. An analysis of the stress contours from ANSYS confirmed expectations of constant stress throughout the tension beams and both tension and compression stresses throughout the bending beams.

PFF Algorithm

1) Design the model of the device to be tested.
2) Apply displacements or forces to the device and record the stress and displacement information for every element in the model.
3) Determine the resistivity of each node from the unidirectional form of the model by multiplying each stress with its corresponding piezoresistive coefficient. Note that σ_1 and σ_2 are the stresses parallel and perpendicular to the current, respectively. Due to the iterative nature of this algorithm, the direction of the current will be updated later on in the process. This process is repeated until the calculated resistance for each iteration stabilizes.
4) Perform an electrical analysis to determine the current through the flexure. Summing the current at the nodes where the voltage is applied gives the total current. This is used in Ohm's law to determine the resistance. If the resistance has changed from the resistance in the previous iteration by more than a predetermined tolerance limit, the process continues to the next step. If not, the resistance is recorded for that load step.
5) Determine the direction of the current. Since the directions of the current, resistivity, and voltage gradient are interdependent, an iterative algorithm must be applied. The voltage gradient can be computed from the electrical analysis. This, in turn, is used to determine the direction of the current. After determining the direction of the current, the algorithm returns to step 3) where the direction of the current is used to determine σ_1 and σ_2 and, hence, the resistivity for each element.
6) All of the preceding steps are completed for each displacement or force value (load step) to complete an analytical data curve.

C. Step 3—Optimization

In the final step, the empirical [step 1)] and analytical [step 2)] data curves are compared in an optimization process to determine the piezoresistive coefficients. The objective of the optimization routine was to minimize the average squared difference between the empirical and analytical data curves. The piezoresistive coefficients (design variables) were varied to yield varying analytical data curves. Each new analytical data curve was compared to the empirical data curve to determine the average squared difference between the curves, which is also known as the fitness value. By using a genetic algorithm, the set of piezoresistive coefficients that yielded the lowest fitness value was determined. A genetic algorithm was used due to the suspected noisiness of the model and because of the number of design variables that was being optimized.

Each set of the design variables in the genetic optimization algorithm makes up a "chromosome." The variables in each chromosome are input into an analytical model. In this case, the analytical model was the PFF algorithm. The output of the model is a resistance-versus-displacement curve that can be compared to a curve from the experimental data. These curves are compared to each other by summing the squared difference at each displacement point to determine a fitness value. The fitness values for several sets of variables are then compared, and the sets of the variables with the worst fit are thrown out. The variables with the best fit are then used to make a new set of variables. This process continues until a standard is achieved. More information about genetic algorithms can be found in [28] and [29].

The most computationally expensive part of the genetic algorithm is using the PFF algorithm for each chromosome. Not only does the PFF algorithm take a considerable time to solve but also the time is multiplied by the number of chromosomes in the set. The time can be reduced by parallel processing, allowing the PFF algorithm to simultaneously compute the analytical data curves for each of the chromosomes in the set. The supercomputers in the Ira and Mary Lou Fulton Supercomputing Laboratory were used for the genetic algorithm parallel processing in this paper. The supercomputer used had 128 MIPS R16000 processors at 700 MHz.

V. OPTIMIZATION RESULTS

Results were generated from the implementation of the reduced model coupled with the optimization algorithm. This process was performed for the two devices shown in Figs. 3 and 4, each in poly 1 and poly 2, resulting in four unique configurations. The optimization routine was designed to find the piezoresistive coefficients that adequately predicted both

TABLE III
REDUCED MODEL PIEZORESISTIVE COEFFICIENTS FOR MUMPS POLY 1 LAYER

π Coeff.	Value	Units
π_{11}	-1.188e-4	MPa^{-1}
π^*_{21}	4.313e-8	MPa^{-2}

TABLE IV
REDUCED MODEL PIEZORESISTIVE COEFFICIENTS FOR MUMPS POLY 2 LAYER

π Coeff.	Value	Units
π_{11}	-1.971e-4	MPa^{-1}
π^*_{21}	1.157e-7	MPa^{-2}

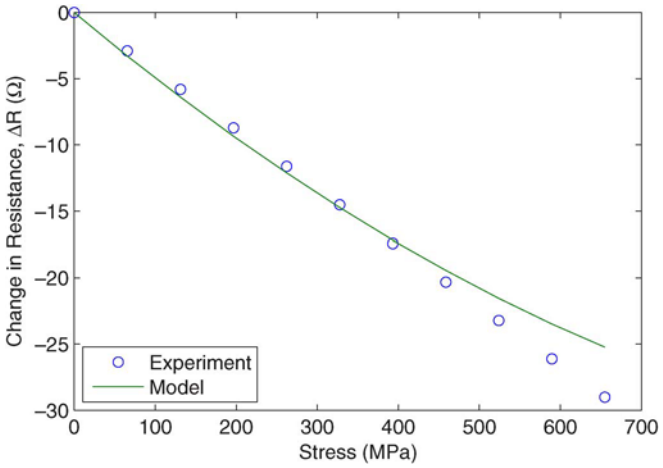

Fig. 9. Experimental data and analytical results for tension microdevice for poly 1. The nominal resistance for this device is 450 Ω.

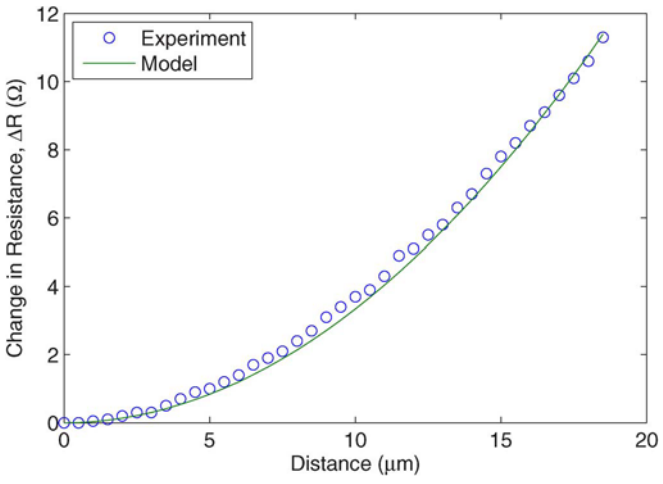

Fig. 10. Experimental data and analytical results for bending microdevice for poly 1. The nominal resistance for this device is 2266 Ω.

tension and bending, simultaneously. Due to the difference in resistivity and thicknesses in poly 1 and poly 2, the optimization routine was run separately for each layer. The optimization found one set of piezoresistive coefficients that adequately described both tension and bending for each given layer. The optimized values for the reduced form of the unidirectional model are listed in Tables III and IV.

The piezoresistive coefficients generated from the optimization routine were used to develop analytical data that are compared to the empirical data, as shown in Figs. 9–12. Figs. 9 and 10 show the comparison between the analytical and empirical data for poly 1, where the analytical data were developed

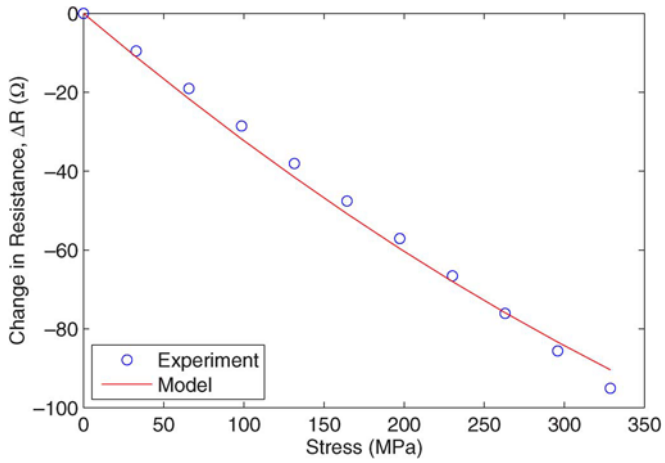

Fig. 11. Experimental data and analytical results for tension microdevice for poly 2. The nominal resistance for this device is 2400 Ω.

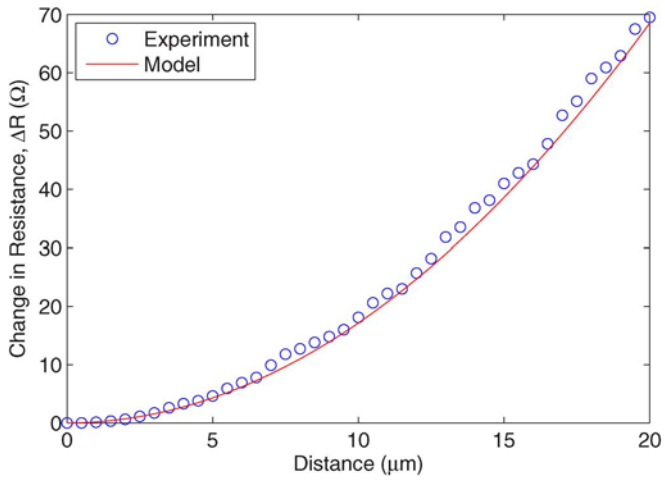

Fig. 12. Experimental data and analytical results for bending microdevice for poly 2. The nominal resistance for this device is 5175 Ω.

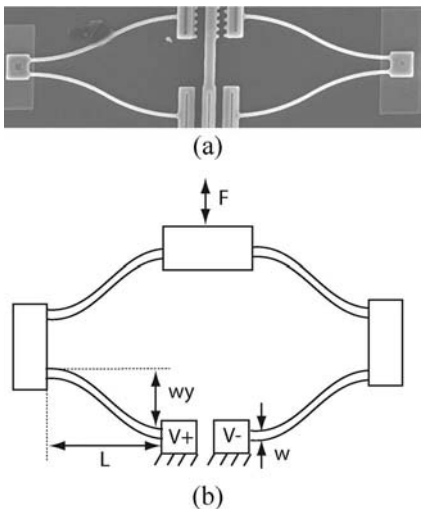

Fig. 13. (a) SEM and (b) schematic of clam microdevice.

TABLE V
DIMENSIONS FOR MICRODEVICES IN THE CASE STUDY ARE GIVEN IN MICROMETERS

Device Name	Fabrication Method	Member Length, L	In-Plane Width, w	Spread Width, wy	Out-of-Plane Thickness, t	Polysilicon Layer
Clam	MUMPs	108	3	29.5	2	1
Ben150p2	MUMPs	150	3	-	1.5	2

using the coefficients in Table III. Figs. 11 and 12 show the comparison between the analytical and empirical data for poly 2 using the coefficients in Table IV. A concave trend can be seen in the analytical tension curves, which varies from the linearity seen in the experimental data. This discrepancy is minimal for a large stress range; however, at high stress levels, it may become more significant. The difference seen in the bending curves is minimal over the test displacement range.

These results show that the unidirectional form of the proposed piezoresistive model can be used to predict the piezoresistive effect due to axial tension and in-plane bending loading of thin isotropic flexures. The same piezoresistive coefficients were used to determine the change in resistance of two devices with varying loading conditions.

VI. CASE STUDY

A case study was done to demonstrate the ability of the model, with the PFF algorithm, to predict the piezoresistive effect. Two devices were used in this case study. The first was the "clam device," shown in Fig. 13, which was fabricated using the poly 1 layer of the MUMPs process. The second was a bending device in the same shape as the device shown in Fig. 4, which was fabricated using the poly 2 layer. Specifications for the devices are given in Table V. The elements and element sizes in Table II resulted in 11 972 elements for a full model of the clam device and 2500 elements for an eighth model of the bending device.

The PFF algorithm prediction was based on the piezoresistive coefficients in Tables III and IV. Empirical data were obtained for the two devices to compare to the predictions from the PFF algorithm. Figs. 14 and 15 show the PFF algorithm predictions compared to the empirical data and predictions from the previous model. The previous model refers to a superposition model using Smith's model implemented in FEA.

The analytical PFF prediction for the clam mechanism follows the general trend of the experimental data. The offset between the two can be explained by several effects, including the two explained here. The piezoresistive coefficients used were determined for initially straight devices, whereas the legs of the clam have an initial curvature. The clam legs are also not as thin and long as the test devices, and these legs are experiencing stresses that were not accounted for in the simplified two-term optimized piezoresistive coefficients. However, the general trend of the prediction follows that of the experimental data, which is not possible with the linear model. This is shown in Fig. 14, which shows the empirical data with the predictions from the PFF algorithm and the predictions using the linear model.

The analytical prediction for the bending device also follows the shape of the experimental data, but it has a better fitness

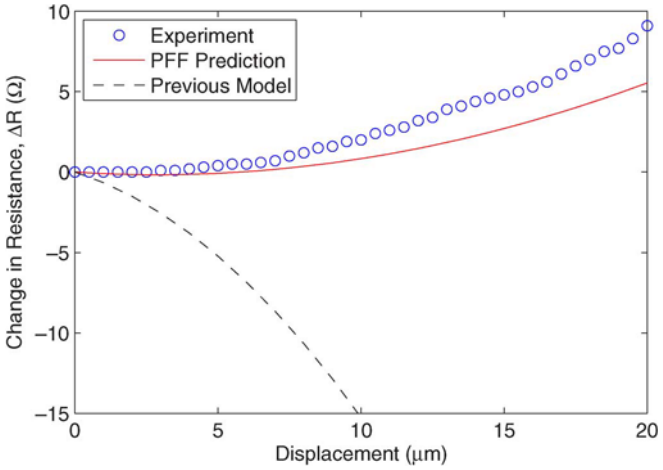

Fig. 14. PFF and linear-model predictions for clam device with a nominal resistance of 2665 Ω.

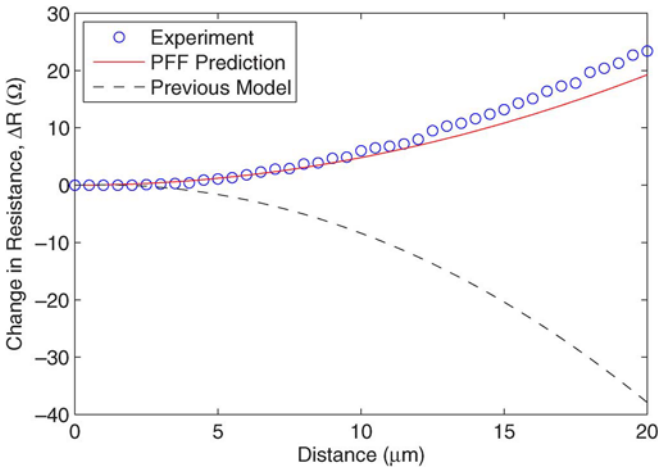

Fig. 15. PFF and linear-model predictions for bending device with a nominal resistance of 7575 Ω.

than the clam device. The difference between the bending device used to obtain the original piezoresistive coefficients and the device used in the PFF algorithm is the length of the legs and the range of stress. The curves match well at lower displacements, yet gradually diverge as the displacement increases. This difference may be due to a slight inaccuracy of the optimized piezoresistive coefficients. Further study may show that a slight change in the second-order coefficient may correct this difference. However, as shown in Fig. 15, the prediction from the PFF algorithm more nearly matches with the data than the prediction from the linear model.

VII. CONCLUSION

The commonly-used linear model of piezoresistivity is based on resistance measurements of beams in pure tension. The

resulting model is valid only for purely tensile or compressive loading. This paper has described a model that uses methods consistent with the previous models but extended to include bending loading conditions. As shown in the results, the model presented in this paper can be used to predict piezoresistivity in n-type polysilicon beams in bending or tension/compression with the same piezoresistive coefficients. The measurements used were based on beams experiencing 2-D bending and beams experiencing tension. As the tension model only applies to uniaxial loading, this model applies only to uniaxial and 2-D bending loading conditions. These loading conditions are the most common for compliant mechanisms and apply to a wide range of microdevices. It is expected that the general model of (5) will predict changes in resistance due to even more complex loading conditions. The experimental results and trends presented are for n-type polysilicon. p-type polysilicon and single crystal silicon will experience a different behavior.

In order for the new model to capture the piezoresistive effect in bending, it had to predict a response with a sign change from the original model. It seems that the piezoresistive effect has a second-order component that is not explained with a linear model. The physics of the piezoresistive effect, including axial loading, are not well understood but would be a valuable research topic for those who study the microstructure of materials.

The development of this model has a potential effect on some commercial FEA programs. Those packages, which use the linear piezoresistive model for resistance change, are adequate for axial loading but will not accurately model resistance changes due to bending. The results of this paper can be implemented by these programs so that future models may accurately model bending effects.

One of the benefits of the new model is the prediction of resistance change for developing integrated compliant microsensors. These microsensors can be fabricated with established MEMS fabrication processes and can be designed to integrate sensing capabilities directly into the geometry of a microdevice. The state of a microdevice can be self-sensed, leading to the possibility of feedback control.

REFERENCES

[1] R. K. Messenger, T. W. McLain, and L. L. Howell, "Feedback control of a thermomechanical inplane microactuator using piezoresistive displacement sensing," *Amer. Soc. Mech. Eng., Dyn. Syst. Control Division (Publication) DSC*, vol. 73, no. 2, pp. 1301–1310, 2004.

[2] R. K. Messenger, T. W. McLain, and L. L. Howell, "Improved nanopositioning resolution through piezoresistive feedback control of a MEMS thermal actuator," *Amer. Soc. Mech. Eng., Dyn. Syst. Control Division (Publication) DSC*, vol. 74, no. 2, pp. 1327–1334, 2005.

[3] R. K. Messenger, T. W. McLain, and L. L. Howell, "Piezoresistive feedback for decreased response time of MEMS thermal actuators," in *Proc. SPIE—Sensors Smart Structures Technologies Civil, Mechanical, Aerospace Systems*, 2006, vol. 6164, p. 6174-06.

[4] J. K. Anderson, "Piezoresistive sensing of bistable micro mechanism state," M.S. thesis, Brigham Young Univ., Provo, UT, 2005.

[5] S. Sze, Ed., *Semiconductor Sensors*. New York: Wiley, 1994.

[6] T. L. Waterfall, "Design of piezoresistive MEMS force and displacement sensors," M.S. thesis, Brigham Young Univ., Provo, UT, 2006.

[7] W. P. Eaton, "Surface micromachined pressure sensors," Ph.D. dissertation, Univ. New Mexico, Albuquerque, NM, 1997.

[8] E. T. Enikov and B. J. Nelson, "MEMS based single cell penetration force sensor," in *Proc. SPIE—Conf. Microrobotics Microassembly*, Boston, MA, Sep. 21–22, 1999, vol. 3834, pp. 40–46.

[9] J. C. Erskine, "Polycrystalline silicon-on-metal strain gauge transducers," *IEEE Trans. Electron Devices*, vol. ED-30, no. 7, pp. 796–801, Jul. 1983.

[10] D. Schubert, W. Jenschke, T. Uhlig, and F. Schmidt, "Piezoresistive properties of polycrystalline and crystalline silicon films," *Sens. Actuators A, Phys.*, vol. 11, no. 2, pp. 145–155, Mar. 1987.

[11] L. L. Howell, *Compliant Mechanisms*. New York: Wiley, 2001.

[12] C. S. Smith, "Piezoresistance effect in germanium and silicon," *Phys. Rev.*, vol. 94, no. 1, pp. 42–49, Apr. 1954.

[13] T. L. Waterfall, G. K. Johns, R. K. Messenger, B. D. Jensen, T. W. McLain, and L. L. Howell, "Observations of piezoresistivity for polysilicon in bending that are unexplained by linear models," *Sens. Actuators A: Phys.,* in press.

[14] G. K. Johns, "The piezoresistive effect in microflexures," M.S. thesis, Brigham Young Univ., Provo, UT, 2007.

[15] J. F. Nye, *Physical Properties of Crystals*. Oxford, U.K.: Oxford Univ. Press, 1985.

[16] A. Amin, "Computer-controlled piezoresistance data-acquisition system," *Rev. Sci. Instrum.*, vol. 60, no. 12, pp. 3812–3817, Dec. 1989.

[17] V. Gridchin, V. Lubimsky, and M. Sarina, "Piezoresistive properties of polysilicon films," *Sens. Actuators A, Phys.*, vol. 49, no. 1/2, pp. 67–72, Jun. 1995.

[18] V. Gridchin and V. Lubimsky, "Phenomenological model of the piezoresistive effect in polysilicon films," *Russ. Microelectron.*, vol. 32, no. 4, pp. 205–213, Jul. 2003.

[19] V. Mosser, J. Suski, J. Goss, and E. Obermeier, "Piezoresistive pressure sensors based on polycrystalline silicon," *Sens. Actuators A, Phys.*, vol. 28, no. 2, pp. 113–132, Jul. 1991.

[20] J. Y. Seto, "Piezoresistive properties of polycrystalline silicon," *J. Appl. Phys.*, vol. 47, no. 11, pp. 4780–4783, Nov. 1976.

[21] O. Tufte and E. Stelzer, "Piezoresistive properties of silicon diffused layers," *J. Appl. Phys.*, vol. 34, no. 2, pp. 313–318, Feb. 1963.

[22] T. Toriyama and S. Sugiyama, "Analysis of piezoresistance in p-type silicon for mechanical sensors," *J. Microelectromech. Syst.*, vol. 11, no. 5, pp. 598–604, Oct. 2002.

[23] P. M. Zavracky, K. Warner, L. Lassic, and J. Green, "Piezoresistivity of silicon-on-insulator films by zone-melting recrystallization," *J. Micromech. Microeng.*, vol. 3, no. 2, pp. 96–101, Jun. 1993.

[24] P. Kleiman, B. Semmache, M. L. Berre, and D. Barbier, "Influence of the structural parameters of polysilicon films on the piezoresistive properties at high temperature," in *Proc. Mater. Res. Soc. Symp.*, 1997, vol. 444, pp. 131–137.

[25] R. E. Beatty, R. C. Jaeger, J. C. Suhling, R. Johnson, and R. D. Butler, "Evaluation of piezoresistive coefficient variation in silicon stress sensors using a four-point bending test fixture," *IEEE Trans. Compon., Hybrids, Manuf. Technol.*, vol. 15, no. 5, pp. 904–914, Oct. 1992.

[26] D. A. Koester, R. Mahadevan, B. Hardy, and K. Markus, *MUMPs Design Handbook*, Cronos Integr. Microsyst., 2002. Rev. 5.0. [Online]. Available: http://www.memsrus.com

[27] J. W. Wittwer, T. Gomm, and L. L. Howell, "Surface micromachined force gauges: Uncertainty and reliability," *J. Micromech. Microeng.*, vol. 12, no. 1, pp. 13–20, Jan. 2002.

[28] L. Davis, *Handbook of Genetic Algorithms*. New York: Van Nostrand Reinhold, 1991.

[29] M. Gen and R. Cheng, *Genetic Algorithms and Engineering Optimization*. New York: Wiley, 2000.

Gary K. Johns received the B.S. and M.S. degrees in mechanical engineering from Brigham Young University, Provo, UT, in 2005 and 2007, respectively.

He is currently with Merit Sensor Systems, Inc., South Jordan, UT, which manufactures piezoresistive pressure sensors. His research efforts were in the area of piezoresistive microsensors.

Larry L. Howell received the B.S. degree from Brigham Young University (BYU), Provo, UT, in 1987, and the M.S. and Ph.D. degrees from Purdue University, West Lafayette, IN, in 1991 and 1993, respectively.

He was a past Chair with the Department of Mechanical Engineering, BYU, where he is currently a Professor. Prior to joining BYU in 1994, he was a Visiting Professor with Purdue University, a Finite Element Analysis Consultant with the Engineering Methods, Inc., and an Engineer on the design of the YF-22 (the prototype for the U.S. Air Force F-22). He is the holder of patents and technical publications which focus on compliant mechanisms and microelectromechanical systems. He is the Author of the book *Compliant Mechanisms* (John Wiley & Sons).

Dr. Howell is a Fellow of ASME, a past Chair of the ASME Mechanisms and Robotics Committee, and an Associate Editor for the *Journal of Mechanical Design*. He is the recipient of the NSF CAREER Award, the ASME Design Automation Conference Best Paper Award, BYU Technology Transfer Award, and the Maeser Research Award.

Brian D. Jensen received the B.S. and M.S. degrees in mechanical engineering from Brigham Young University, Provo, UT, in 1996 and 1998, respectively, and the M.S. degree in electrical engineering and Ph.D. degree in mechanical engineering from the University of Michigan, Ann Arbor, in 2004.

In 1998 and 1999, he spent 16 months as a Micromechanism Designer with Sandia National Laboratories, Albuquerque, NM. He is currently with Brigham Young University, Provo, UT. He has performed research and published over 40 papers in a wide variety of design topics, including microelectromechanical systems and compliant mechanisms. He is the holder of seven U.S. patents.

Dr. Jensen was the recipient of a National Science Foundation Graduate Research Fellowship and a Department of Defense Science and Engineering Graduate Fellowship.

Timothy W. McLain (S'91–M'93–SM'05) received the B.S. and M.S. degrees from Brigham Young University (BYU), Provo, UT.

He worked for two years with Sarcos, Inc., Salt Lake City, UT, on the control of fluid-power systems for robotics applications. While completing his Ph.D. degree work with the Stanford University, Stanford, CA, he worked with the Monterey Bay Aquarium Research Institute on the control of underwater robotic vehicles. Since 1995, he has been with BYU, where he is currently a Professor and the Department Chair with the Mechanical Engineering Department. During the summer of 1999 and 2000, he was a Visiting Scientist with the Air Force Research Laboratory. Since that time, he has pursued a research involving control and planning for miniature unmanned aerial vehicles. He has also been involved in the modeling and control of microelectromechanical systems.

Dr. McLain is a Senior Member of AIAA and is a member of the AIAA Unmanned Systems Program Committee.